Rostock. Math. Kolloq. **49**, 163–184 (1995)

Subject Classification (AMS)
Primary 76E30;
Secondary 58F12

Peter Takáč

Dynamics on the Attractor for the Complex Ginzburg-Landau Equation[1]

Dedicated to the professors of mathematics
L. Berg, W. Engel, G. Pazderski, *and* H.- W. Stolle.

ABSTRACT. We present a numerical study of the large-time asymptotic behavior of solutions to the one-dimensional complex Ginzburg-Landau equation with periodic boundary conditions. Our parameters belong to the Benjamin-Feir unstable region. Our solutions start near a pure-mode rotating wave that is stable under sideband perturbations for the Reynolds number R ranging over an interval (R_{sub}, R_{sup}). We find sub- and super-critical bifurcations from this stable rotating wave to a stable 2-torus as the parameter R is decreased or increased past the critical value R_{sub} or R_{sup}. As $R > R_{sup}$ further increases, we observe a variety of dynamical phenomena, such as a local attractor consisting of three unstable manifolds of periodic orbits or 2-tori cyclically connected by manifolds of connection orbits. We compare our numerical simulations to both rigorous mathematical results and experimental observations for binary fluid mixtures.

KEY WORDS. Periodic orbit; 2- and 3-tori; stability; local attractor; psedo-spectral method; Fourier modes

1 Introduction

An important tool in the theory of phase transitions and instability waves is the time-dependent complex Ginzburg-Landau equation (CGL, for short)

$$\partial_t A = (1 + i\nu)\partial_{xx}^2 A + (R - (1 + i\mu)|A|^2)A, \quad -\infty < x < \infty,\ t \geq 0, \tag{1}$$

[1]This work was supported in part by the Applied Mathematical Sciences subprogram of the Office of Energy Research, United States Department of Energy, under Contract W-31-109-Eng-38 through Argonne National Laboratory. The author expresses his appreciation to the Mathematics and Computer Science Division at Argonne National Laboratory for the hospitality during his 1990–91 academic leave.

where x and t are the spatial and temporal variables, respectively, and the unknown complex-valued function $A(x,t)$ represents an order parameter or a wave function. Here, μ, ν and $R \in (-\infty, \infty)$ are parameters. Originally discovered by GINZBURG AND LANDAU [6] for a phase transition in superconductivity, this equation was subsequently derived for instability waves in hydrodynamics such as the nonlinear growth of RAYLEIGH-BÉNARD convective rolls (NEWELL AND WHITEHEAD [17]), the appearance of TAYLOR vortices in the COUETTE flow between counter-rotating cylinders (STUART AND DI PRIMA [21]), and the development of TOLLMIEN-SCHLICHTING waves in plane POISEUILLE flows (BLENNERHASSETT [1]). Also instability waves for perturbation concentration in chemically reacting and diffusing systems are described by the CGL equation (KURAMOTO AND TSUZUKI [12]). In these applications, Eq. (1) describes the small and slowly varying (in space and time) amplitude and phase of a mode that bifurcates via an oscillatory instability from a homogeneous basic state (NEWELL [16]). The parameter R corresponds to a REYNOLDS number; we use it as the bifurcation (or control) parameter. We impose periodic boundary conditions

$$A(x+1,t) = A(x,t), \quad -\infty < x < \infty,\ t \geq 0. \tag{2}$$

For example, periodic boundary conditions are appropriate for experiments with RAYLEIGH-BÉNARD convective rolls in a binary fluid mixture contained in a cell of annular geometry, where the complex amplitude $A(x,t)$ describes the wave moving along the boundary between two concentric convective rolls, cf. JANIAUD ET AL. [8, 9]. The oscillatory instability of the two convective rolls develops as the control parameter R increases and crosses a critical value $R_0 > 0$. At $R = R_0$ the boundary between the two concentric rolls is a circle. A generic point on this circle is determined by its azimuthal angle θ, $0 \leq \theta < 2\pi$. Hence $x = \theta/2\pi$ in Eqs. (1, 2). For $R > R_0$ near R_0, after a transient, a wave rotating either clockwise or counter-clockwise settles along the circular boundary between the two rolls. The complex amplitude $A(x,t)$ of this *rotating wave* is a solution of Eqs. (1, 2) given by

$$A(x,t) = a_n e^{i(k_n x - \omega_n t)}, \quad n = 0, \pm 1, \pm 2, \cdots, \tag{3}$$

where $k_n = 2n\pi$ is the wavenumber of the annular spatial pattern with $|n|$ wavelengths, a_n is a complex constant satisfying $|a_n|^2 = R - k_n^2$, and $\omega_n = \mu R + (\nu - \mu)k_n^2$. The real constants μ and ν are determined by measuring the angular frequency ω_n for several values of R. As R further increases from $R_0 \equiv R_{0,n}$ and crosses a critical value $R_1 \equiv R_{1,n} > R_0$, the spatial pattern of the rotating wave starts to exhibit an *amplitude modulation* of the form

$$|A(x,t)| = a(x - ct), \quad a \not\equiv \text{const}, \tag{4}$$

with a second frequency $c \equiv c(R)$ near $c_n = c(R_1) \neq 0$ for $R > R_1$ near R_1. This temporally *biperiodic pattern* is characterized by the complex wave function

$$A(x,t) = (1 + U(x-ct))a_n e^{i[k_n(x-ct)-\omega t]} \equiv V(x-ct)e^{-i\omega t}, \tag{5}$$

where U is a small relative perturbation of the rotating wave $a_n e^{i[k_n(x-ct)-\omega t]}$ and ω is a small perturbation of ω_n, for $R - R_1 > 0$ small (cf. Takáč [22]).

In our numerical simulations we fix the constants $\mu = -1$ and $\nu = 5$, and thus, by the NEWELL criterion [15], we are in the BENJAMIN-FEIR *unstable* region $1 + \mu\nu < 0$. We focus on the large-time asymptotic behavior of the solutions $A(x,t)$ to Eqs. (1, 2) starting from an initial distribution $A(x,0)$ near the rotating wave (3) for $n = 1$. In particular, we investigate the sideband instability of this rotating wave, cf. ECKHAUS [5]. We have performed numerical simulations for a large range of values of the bifurcation parameter $R \in (0,\infty)$. We report here only those cases which clearly exhibit local attractors of special interest. For particular values of R, we have obtained stable rotating waves, 2-tori, and periodic orbits that have a temporally constant modulus which becomes time-periodic as R passes a critical value. We determine several critical values of R at which a bifurcation from a stable periodic orbit to a stable 2-torus takes place. We have also obtained local attractors consisting of two or three unstable manifolds of periodic orbits or 2-tori cyclically connected by manifolds of connection orbits, where the manifolds of periodic orbits or 2-tori have distinct dimensions. We compare these periodic orbits and 2-tori with those ones previously obtained by rigorous analysis and/or numerical simulations, cf. NEWTON AND SIROVICH [18, 19], SIROVICH AND NEWTON [20], and TAKÁČ [22]. This comparison provides some analytic background for our numerical simulations. We emphasize that our simulations using periodic boundary conditions (2) are different from those performed in MOON ET AL. [14], KEEFE [10], and DOELMAN [3] with Neumann boundary conditions. Since we are also interested in the *stability* of the solutions to Eq. (1) in a suitable Banach or Hilbert space of smooth 1-periodic functions $f\colon \mathbb{R} \to \mathbb{C}$, we do *not* presuppose any *special form* of these solutions. The numerical simulations presented in this article are the first ones studying the stability of 2-tori for the full system (1, 2). As usual, we write $\mathbb{R} = (-\infty,\infty)$ and $\mathbb{C} = \mathbb{R} \oplus i\mathbb{R}$ to denote the real line and the complex plane, respectively.

Our numerical integration of the evolution equation (1) uses a pseudo-spectral method (PSM, for short) for sufficiently long time (from $t = 0$ up to $t = 1000$). This PSM consists of an approximation by FOURIER series in space (with $-N^{\text{th}}$ through N^{th} FOURIER modes, $N = 15$, 31 and 63) combined with a fourth-order RUNGE-KUTTA discretization in time (with the time step $h = 0.0001$, 0.0002 and 0.0005). We have implemented this method on an Ardent Titan Supercomputer with four parallel processors using a FORTRAN code with both vector and parallel optimizations. All computations have been carried out in double precision complex arithmetics.

This article is organized as follows. In Section 2 we study bifurcations from rotating waves (3) to the 2-tori (5) together with their stability. In Section 3 we observe certain periodic orbits that have a temporally constant modulus which becomes time-periodic as R passes a critical value. In Section 4 we obtain local attractors consisting of two or three unstable manifolds of periodic orbits or 2-tori cyclically connected by manifolds of connection orbits. Finally, Section 5 contains a discussion.

2 Bifurcations from Rotating Waves

In this section we investigate bifurcations from stable rotating waves of the form (3) to the 2-tori (5) together with the exchange of stability, for $n = 1$. We find a *stable* 2-torus (5) for $137.9 \le R \le 139.7$ which bifurcates *supercritically* from a stable rotating wave (3). A perturbation of the rotating wave (3) can be written as

$$A(x,t) = (1 + B(x,t))a_n e^{i(k_n x - \omega_n t)}, \tag{6}$$

where B is small enough. The sideband instability analysis is carried out by inserting Eq. (6) into (1) and retaining only the terms of the first order in B (cf. Doering et al. [4] or Takáč [22]):

$$\partial_t B = (1 + i\nu)\partial^2_{xx} B + 2i(1 + i\nu)k_n \partial_x B - (1 + i\mu)|a_n|^2(B + B^*), \tag{7}$$

where $|a_n|^2 = R - k_n^2$. The asterisk * denotes the complex conjugate. The sideband stability of the zero solution of Eq. (7) to perturbations of a discrete wavenumber $k_m = 2\pi m$, $m = \pm 1, \pm 2, \cdots$, is determined by writing

$$B(x,t) = b^+(t)e^{ik_m x} + (b^-(t))^* e^{-ik_m x}. \tag{8}$$

The evolution equations for the complex amplitudes $b^+(t)$ and $b^-(t)$ have the form

$$\frac{d}{dt}\begin{pmatrix} b^+ \\ b^- \end{pmatrix} = -\begin{pmatrix} C^+ & (1 + i\mu)|a_n|^2 \\ (1 - i\mu)|a_n|^2 & (C^-)^* \end{pmatrix}\begin{pmatrix} b^+ \\ b^- \end{pmatrix} \tag{9}$$

where

$$C^\pm = (1 + i\nu)k_m^2 \pm 2(1 + i\nu)k_m k_n + (1 + i\mu)|a_n|^2. \tag{10}$$

The *neutral stability curves* (R, k_n^2) for the zero solution of Eq. (9) satisfy the relation (cf. [4, 22])

$$4k^2\left[1 + \left(\frac{\nu k_m^2 + \mu(R - k^2)}{k_m^2 + R - k^2}\right)^2\right] = 2(1 + \mu\nu)(R - k^2) + (1 + \nu^2)k_m^2 \tag{11}$$

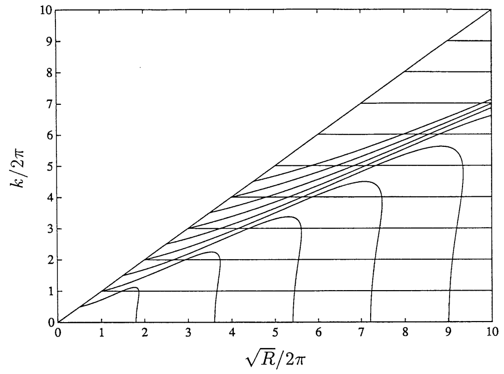

Figure 1: Neutral stability curves in the $(R^{1/2}, k)$-plane for the parameter values $(\mu, \nu) = (-1, 5)$.

where the continuous variable k replaces the discrete wavenumber $k = k_n$. For $(\mu, \nu) = (-1, 5)$ these curves are plotted in the $(\sqrt{R}, k)$-plane in Fig. 1. Each curve corresponds to a fixed value of $|m| = 1, 2, \cdots$. For a fixed value of $R > 0$, the rotating wave (3) is stable to sideband perturbations (8) if and only if exactly one solution k of Eq. (11) satisfies $k > |k_n|$. In particular, the rotating wave for $n = 1$ is stable to *all* sideband perturbations if and only if the REYNOLDS number R belongs to an interval (R_{sub}, R_{sup}). From a magnification of the graph in Fig. 1 (cf. TAKÁČ [22]) for $m = n = 1$, we have found the numerical values (precise up to computer round-off errors)

$$R_{sub} = 84.96 \quad \text{and} \quad R_{sup} = 137.90. \tag{12}$$

The existence and uniqueness (up to shifts in space and time) of the 2-tori having the form (5) has been proved by TAKÁČ [22] using bifurcation theory for $R_{sub} - R > 0$ and $R - R_{sup} > 0$ small enough. The second frequency $c = c_n$ for the critical values $R = R_{sub}$ and $R = R_{sup}$ can be computed in a similar way as the neutral stability curves. We insert Eq. (5) into (1) and retain only the terms of first order in U (cf. TAKÁČ [22])

$$(1 + i\nu)U'' + (c_n + 2i(1 + i\nu)k_n)U' - (1 + i\mu)|a_n|^2(U + U^*) = 0, \tag{13}$$

where $|a_n|^2 = R - k_n^2$. This equation has a nonzero solution of the form

$$U(x) = b^+ e^{ik_m x} + (b^-)^* e^{-ik_m x} \tag{14}$$

if and only if the linear system

$$\begin{pmatrix} C^+ - ik_m c_n & (1 + i\mu)|a_n|^2 \\ (1 - i\mu)|a_n|^2 & (C^-)^* - ik_m c_n \end{pmatrix} \begin{pmatrix} b^+ \\ b^- \end{pmatrix} = 0 \tag{15}$$

has a nonzero solution, where $C^{\pm}$ is defined by Eq. (10). This is the case if and only if R satisfies Eq. (11) and

$$c = 2k(\nu - \mu)\frac{R - k^2}{k_m^2 + R - k^2}. \tag{16}$$

The numerical values (12) for $m = n = 1$ yield the respective frequencies

$$c_{sub} = 40.36 \quad \text{and} \quad c_{sup} = 53.81. \tag{17}$$

To study the stability of the 2-tori from Eq. (5) we have used numerical integration of the evolution equation (1). Applying our pseudo-spectral method (PSM, for short, described in Section 1) for sufficiently long time (from $t = 0$ up to $t = 1000$), we have obtained the following numerical results for $\mu = -1$ and $\nu = 5$:

2.1 A supercritical bifurcation at $R = R_{sup}$

The numerical value of R_{sup} obtained by PSM coincides with its value from (12) within the indicated precision, $R_{sup}^{num} = 137.9$. For $R = R_{sup}^{num}$ the numerical solution of (1) slowly looses all Fourier modes except for the first one, thus converging towards the pure-mode rotating wave (3) with $n = 1$. Various initial values at $t = 0$ led to a fast transition before $t = 1$ into a state with the first Fourier mode more than 10^3-times larger than the remaining ones which also decayed exponentially with the increasing wavenumber. The decay of these sideband Fourier modes ($n \neq 1$) then slowly continued throughout the entire evolution ($0 \leq t \leq 1000$). On the other hand, for $R = 138.0$ a similar transition was observed, but after $t = 1$ the decaying sideband modes started to settle away from zero until $t = 100$ when their decay ceased completely. The first mode was on the order of 10^5-times larger than the zeroth and second modes. From the graph of the amplitude modulation (4) the frequency c was found to be $c_{sup}^{num} = 1/0.0186 = 53.76$. Increasing R up to the value $R = 139.7$ we observe increasing sideband modes. The amplitudes of these modes are constant in time with nearly linear logarithmic decay (Fig. 2(a)). The graph of the amplitude modulation (4) in Fig. 2(b) gives the frequency $c = 1/0.0194 = 51.55$ at $R = 139.7$. For $137.9 \leq R \leq 139.7$ the stability of this temporally biperiodic motion (2-torus) was tested by various small perturbations. At $R = 139.8$ this 2-torus becomes unstable. The zeroth Fourier mode slowly increases and becomes the dominant one. Eventually the amplitudes of all modes become constant in time with nearly linear logarithmic decay again (Fig. 3(a)). The graph of the amplitude modulation (4) in Fig. 3(b) is time-independent ($c = 0$). During the transition from a 2-torus to a limit-cycle, the amplitude (4) decreases to zero at one point where a phase slip occurs.

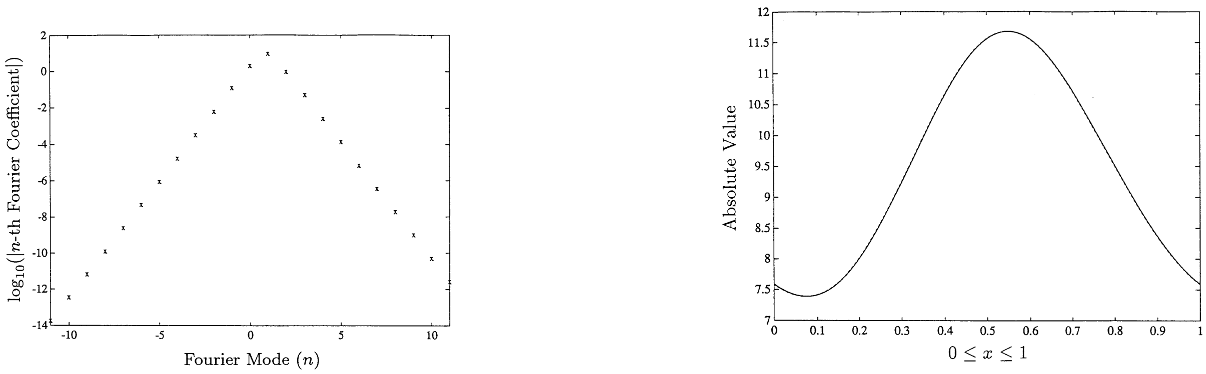

Figure 2: For $R = 139.7$, (a) logarithmic decay of Fourier modes; (b) amplitute modulation.

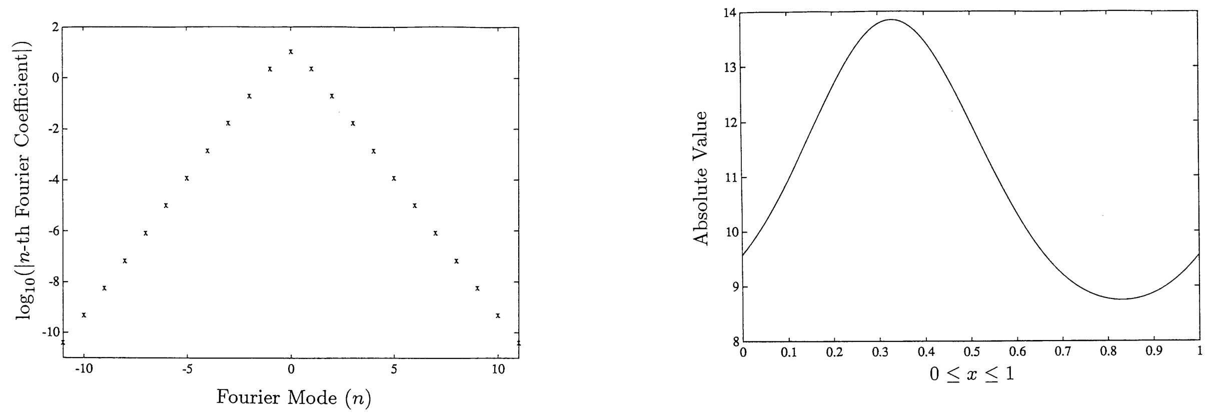

Figure 3: For $R = 139.8$, (a) logarithmic decay of Fourier modes; (b) amplitude modulation.

2.2 A subcritical bifurcation at $R = R_{sub}$

The numerical value of R_{sup} obtained by PSM differs from its value from (12), $R_{sub}^{num} = 84.99$. Similarly to the case $R = R_{sup}^{num}$, for $R = R_{sub}^{num}$ the numerical solution of (1) slowly looses all FOURIER modes except for the first one, thus converging towards the pure-mode rotating wave (3) with $n = 1$. For $R = 84.98$ a stable 2-torus (5) was observed with $c_{sub}^{num} = 1/0.0248 = 40.32$. At $R = 84.97$ this 2-torus becomes unstable. Again, the zeroth FOURIER mode slowly increases and becomes the dominant one with the remaining FOURIER modes approaching zero, and thus the rotating wave (3) with $n = 0$ is obtained.

To summarize the results of this section, we have found a *stable* 2-torus (5) for $137.9 \leq R \leq 139.7$ which bifurcates *supercritically* from a stable rotating wave (3) for $n = 1$. Although several previous articles [2, 8, 9, 11, 13] studied solutions similar to (5), their stability under the temporal evolution was not known.

3 Bifurcations from Some Periodic Orbits

In this section we are concerned with primary and secondary bifurcations from the STOKES *wave* $A(x,t) = a_0 e^{-i\omega_0 t}$ which is the special case of a rotating wave (3) for $n = 0$. In the next section we will need these bifurcations in order to be able to explain the dynamics on some local attractors for the CGL equation. Some analytic and computational background for these simulations can be found in NEWTON AND SIROVICH [18, 19] and SIROVICH AND NEWTON [20]. Therefore we present here only those results that are either new or necessary for a proper understanding of the next section. The reader is referred to GUCKENHEIMER AND HOLMES [7] for general facts about dynamical systems and bifurcations.

3.1 Separable periodic orbits

We begin with the stability of the STOKES wave for $(\mu,\nu) = (-1,5)$. Similarly as in the previous section, the STOKES wave ($n = 0$) is stable to *all* sideband perturbations if and only if the REYNOLDS number R belongs to an interval $(0, R_I)$, where

$$R_I = -2\pi^2(1+\nu^2)/(1+\mu\nu) \doteq 128.3049 \tag{18}$$

is the value of R satisfying Eq. (11) for $k = 0$ and $m = \pm 1$, see Fig. 1. According to NEWTON AND SIROVICH [18], as the parameter R crosses R_I, the STOKES wave bifurcates to another periodic orbit of the separable form

$$A(x,t) = F(x)e^{-i\Omega t}. \tag{19}$$

Here Ω is a real number, and $F\colon \mathbb{R} \to \mathbb{C}$ is a 1-periodic function satisfying

$$(1+i\nu)F'' + (R + i\Omega - (1+i\mu)|F|^2)F = 0, \quad -\infty < x < \infty, \tag{20}$$

by (1, 2) and (19). Our numerical simulations show that the periodic orbit (19) is stable for all R from an interval (R_I, R_{II}), where we have observed the value

$$R_{II} = 162.4. \tag{21}$$

In particular, we have $F \not\equiv \mathrm{const}$. As R crosses R_{II}, the periodic orbit (19) loses its stability and bifurcates to a stable 2-torus. An analytic approximation of the value R_{II} is presented in NEWTON AND SIROVICH [19]. More precisely, we have obtained a local attractor $\mathcal{A}$ of real dimension 2 consisting of all functions $f\colon \mathbb{R} \to \mathbb{C}$ such that

$$f(x) = F(x - x_0)e^{i\Omega t_0} \quad \text{for some} \quad x_0, t_0 \in \mathbb{R}. \tag{22}$$

Hence, $\mathcal{A}$ is a 2-torus. Furthermore, for all

$$R \in (139.7, R_{II}) = (139.7, 162.4)$$

(see §2.1 and (21) above), our simulations show that the solutions $A(x,t)$ to Eqs. (1, 2) starting from an initial distribution $A(x,0)$ near the rotating wave (3) for $n = 1$ are attracted to $\mathcal{A}$.

3.2 2-tori with periodic modulus

As R increases past the critical value R_{II}, the separable periodic orbit (19) bifurcates *supercritically* to a 2-torus. Our simulations show that also *exchange of stability* takes place. The corresponding stability analysis for this bifurcation has been carried out in Sirovich and Newton [20]. The 2-torus has the form

$$A(x,t) = (F(x) + G(x,t))e^{-i\Omega t} \equiv \Phi(x,t)e^{-i\Omega t}, \tag{23}$$

where the perturbation function $G\colon \mathbb{R} \times \mathbb{R} \to \mathbb{C}$ takes small values for $R - R_{II} > 0$ small, and it is 1-periodic in x and τ-periodic in t, for some $\tau > 0$. The half-period $\tau/2$ coincides with the time-period of the zeroth Fourier mode of the square modulus $|A(x,t)|^2 = |\Phi(x,t)|^2$. As this mode is always real and nonnegative, τ can easily be determined from the graph of this mode versus the time t. For all

$$R \in (R_{II}, R_{II} + 0.1) = (162.4, 162.5),$$

we have observed approximately the same value of τ,

$$\tau_{II} = 1.23. \tag{24}$$

The 2-torus (23) then remains stable for all values $R \in (R_{II}, 180.0]$. More precisely, we have obtained a local attractor $\mathcal{A}$ of real dimension 3 consisting of all functions $f\colon \mathbb{R} \to \mathbb{C}$ such that

$$f(x) = \Phi(x - x_0, -t_1)e^{i\Omega t_0} \quad \text{for some} \quad x_0, t_0, t_1 \in \mathbb{R}. \tag{25}$$

Hence, $\mathcal{A}$ is a 3-torus. Furthermore, for all

$$R \in (R_{II}, 180.0] = (162.4, 180.0],$$

our simulations show that the solutions $A(x,t)$ to Eqs. (1, 2) starting from an initial distribution $A(x,0)$ near the rotating wave (3) for $n = 1$ are attracted to $\mathcal{A}$.

It is remarkable that the angular frequency Ω in both cases (19) and (23) *stays near* the angular frequency of the Stokes wave

$$\omega_0 = \mu R + (\nu - \mu)k_0^2 = -R$$

with a relative error of less than 1.5%, for all $R \in (R_I, 180.0] = (128.3, 180.0]$.

3.3 A 2-torus with periodic modulus for $R = 180.0$

Now we will closer examine a transparent case of a 2-torus (23) for $R = 180.0$. We write

$$A(x,t) = r(x,t)e^{i[\theta(x,t) - \omega_0 t]}, \tag{26}$$

where $r(x,t) = |A(x,t)|$, $\theta(x,t) \in \mathbb{R}$, and $\omega_0 = -180.0$ is the angular frequency of the STOKES wave. In our figures below we limit the values of the phase angle $\theta(x,t)$ to the interval $(-\pi, \pi]$, thus admitting jumps of size $\pm 2\pi$ in the values of $\theta(x,t)$. Given a real function $f(x,t)$, we make its 3-dimensional plot as follows. The origin of our coordinate system is in the middle of the left side of our window, the axis x (axis t, respectively) runs from the origin towards the right lower (right upper) corner, and the values of f are plotted on the vertical axis.

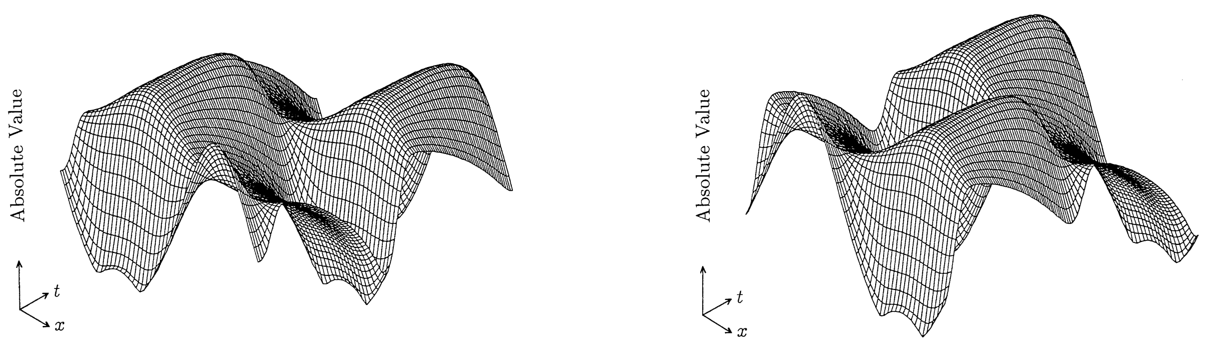

Figure 4: For $R = 180.0$, the modulus $|A(x,t)|$ for (a) $0 \le t \le 0.116$; (b) $0.058 \le t \le 0.174$.

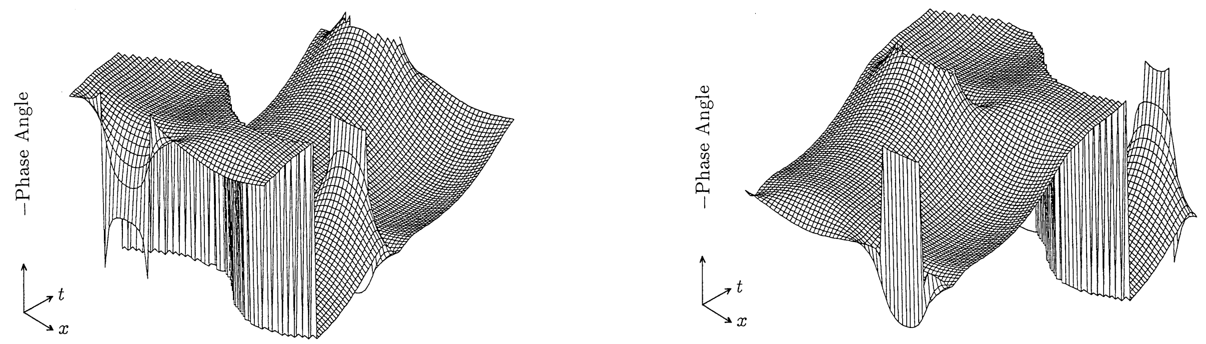

Figure 5: For $R = 180.0$, the negative phase angle $-\theta(x,t)$ for (a) $0 \le t \le 0.116$; (b) $0.058 \le t \le 0.174$.

By (23), the modulus $r(x,t)$ is 1-periodic in x and τ-periodic in t. The graphs of $r(x,t)$ for $(x,t) \in [0,1] \times [0,\tau]$ and $(x,t) \in [0,1] \times [\tau/2, 3\tau/2]$, respectively, are plotted in Fig. 4(a,b). From magnifications of these plots we have obtained the period $\tau = 0.116$. Analogously, the graphs of the negative phase angle $-\theta(x,t)$ are plotted in Fig. 5(a,b). Again, from magnifications of these plots we have deduced that the relative error

$$\frac{|\Omega - \omega_0|}{|\omega_0|} = \frac{|\theta(x, t+\tau) - \theta(x,t)|}{|\omega_0|\tau}$$

is less than 1.5%. We will derive this estimate also from the following study of the complex FOURIER modes $c_n(t)$ of the function $A(x,t)$ of $x \in [0,1]$.

It follows from (23) that $c_n(t)e^{i\Omega t}$ is a τ-periodic function of t. In Fig. 6(a,b) we plot the trajectories of the functions $c_n(t)e^{i\omega_0 t}$ $(0 \le t < 25\tau)$ in the complex plane for each $n = 0$ and $n = 1$, respectively. The phase angle of the function

$$c_n(t)e^{i\Omega t}/c_n(t)e^{i\omega_0 t} = e^{i(\Omega - \omega_0)t}$$

is equal to $(\Omega - \omega_0)t$. By (an animation leading to) Fig. 6(b), it takes approximately 21 time-periods of length τ for this angle to increase or decrease from 0 to $\pm 2\pi$. Thus, the relative difference between Ω and ω_0 can be estimated by

$$\frac{|\Omega - \omega_0|}{|\omega_0|} \le \frac{2\pi}{21\tau|\omega_0|} = \frac{2\pi}{21 \cdot 0.116 \cdot 180.0} < 0.015.$$

Consequently, the period $2\pi/|\Omega| \doteq 2\pi/180 \doteq 0.035$ corresponding to Ω is more than 3-times smaller than $\tau = 0.116$.

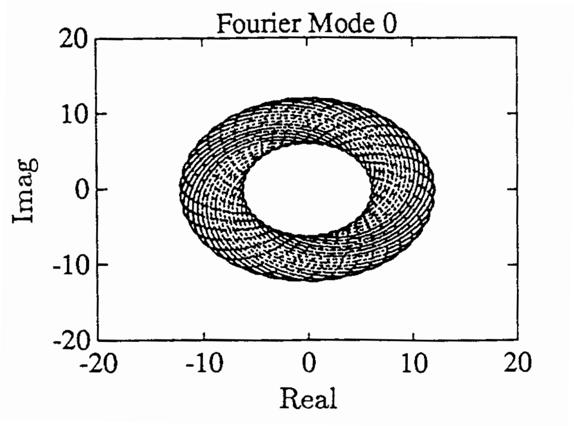

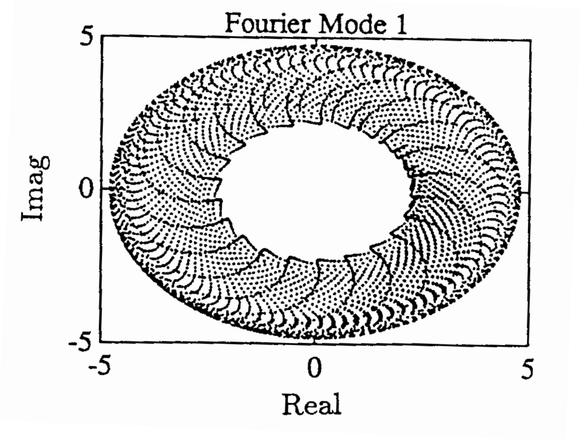

Figure 6: For $R = 180.0$, the complex plots of $c_n(t)e^{i\omega_0 t}$ $(0 \le t < 2.9)$ for (a) $n = 0$; (b) $n = 1$.

To summarize the results of this section, we have found a *stable* 2-torus (23) for $162.4 < R \le 180.0$ which bifurcates *supercritically* from a stable periodic orbit (19) at $R_{II} = 162.4$.

4 A Few Complicated Local Attractors

We have observed that the 2-torus (23) collapses as R is increased from 180.0 to 181.0. We have not detected any signs of a bifurcation from this stable 2-torus to a stable 3-torus for $R \in (180.0, 181.0)$. What we have detected for a number of values of $R \in [181.0, 185.0]$ is an interesting *local attractor* which we analyze below.

4.1 A local attractor for $R = 185.0$

We start our simulations from an initial distribution $A(x, t_0)$ near the rotating wave (3), where $n = 1$, $k_1 = 2\pi$,

$$|a_1| = (185.0 - (2\pi)^2)^{1/2} \doteq 12.0632, \tag{27}$$

and $\omega_1 = -185.0 + 6 \cdot (2\pi)^2 \doteq 51.8701$. For a later comparison, the period τ_1 corresponding to the angular frequency ω_1 has the value

$$\tau_1 = 2\pi/\omega_1 \doteq 0.1211. \tag{28}$$

After a transient time interval of 2 units we set our time variable t to $t = 0$ (i.e. $t_0 = -2$) and begin our observations. Our simulations show that the modulus $|A(x,t)|$ remains both spatially and temporally constant for a relatively long time,

$$|A(x,t)| = 12.063 \quad \text{for all} \quad x \in [0,1] \;\text{ and }\; t \in [0, 0.37].$$

Examining also the phase angle $\theta(x,t)$ from (26), we conclude that $A(x,t)$ is very close to the rotating wave (3) with $n = -1$, for all $t \in [0, 0.37]$, see (27).

As the time t increases past 0.37, the instability of the rotating wave causes both spatial and temporal deviations of the modulus $|A(x,t)|$ from the value 12.063. By Fig. 7(a,b), these deviations have the form of an increasing travelling wave with a sine-like shape moving from the right to the left with the velocity $c_{-1} = -61$ (approximately). Although the present parameter $R = 185.0$ is far beyond the bifurcation value $R_{sup} = 137.90$ from (12), formula (16) from our instability analysis in Section 2 yields a comparable value of the velocity (for $m = \pm 1$, $n = -1$)

$$\hat{c}_{-1} = 2 \cdot (-2\pi) \cdot 6 \cdot \frac{185.0 - (2\pi)^2}{185.0} \doteq -59.31.$$

The deviations continue to increase up to $t = 0.744$ when a phase slip occurs at $x = 0.40$ where $A(x,t) = 0$, see Fig. 8(a,b). After this moment, $A(x,t)$ starts approaching a 2-torus apparently having the form (23). This 2-torus can clearly be seen for $0.80 \le t \le 0.95$ in

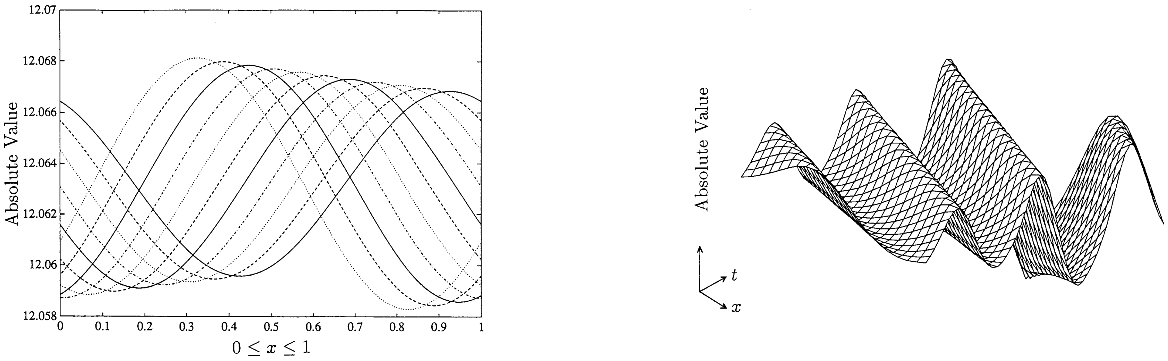

Figure 7: For $R = 185.0$, the deviations $|A(x,t)| - 12.063$ for (a) $0.49 \leq t \leq 0.50$; (b) $0.70 \leq t \leq 0.75$.

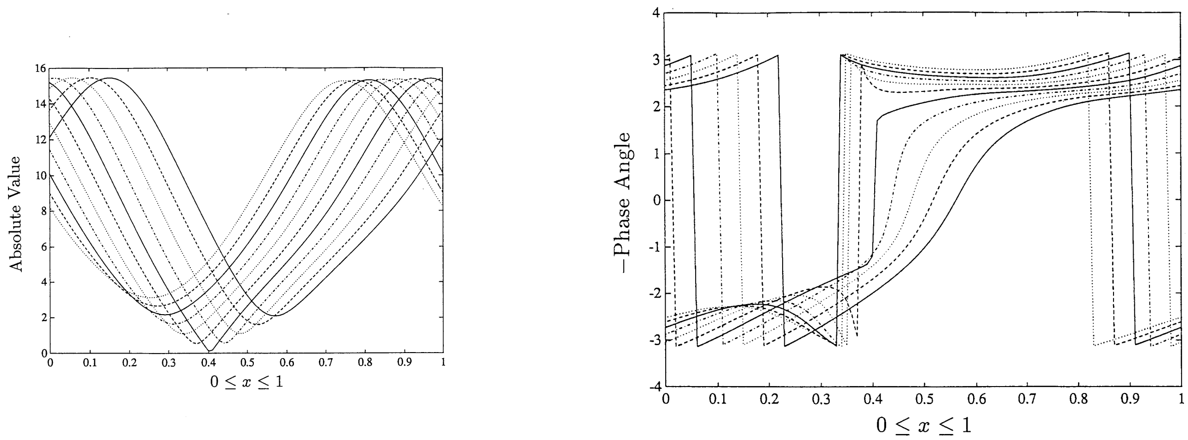

Figure 8: The phase slip for $R = 185.0$, (a) modulus; (b) negative phase angle.

Fig. 9(a,b). It is very similar to the 2-torus in Fig. 4(a,b), but its period $\tau = 0.06$ is about twice smaller than in the latter case ($\tau = 0.116$).

As the time t increases past 0.95, the instability of the 2-torus becomes visible. For $0.95 \leq t \leq 1.06$ we observe a connection orbit from this 2-torus towards a periodic orbit having the form (19), see Fig. 10(a,b) for the modulus $|A(x,t)|$. This modulus remains temporally constant for all $t \in [1.06, 1.29]$ (Fig. 11(a)). It has a shape close to that of the function $|\sin k_1(x - x_0)|$, where $k_1 = 2\pi$ and $x_0 = 0.31$. Inspecting also the negative phase angle $-\theta(x,t)$ defined in (26) (Fig. 11(b)), we conclude that $A(x,t)$ has a form close to

$$A_1(x,t) = \varepsilon e^{-i\Omega t} \sin k_1(x - x_0), \tag{29}$$

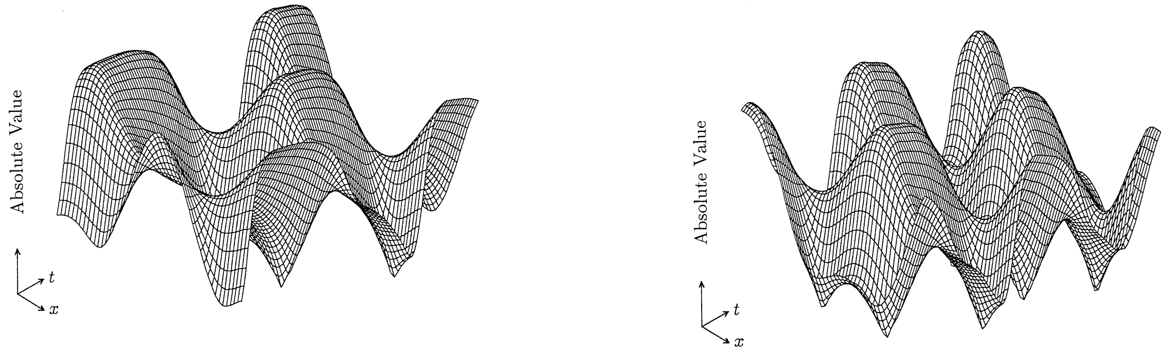

Figure 9: For $R = 185.0$, the modulus $|A(x,t)|$ for (a) $0.80 \le t \le 0.90$; (b) $0.90 \le t \le 1.00$.

where $|\varepsilon| = 14.0$ and

$$\Omega = \omega_0 - \frac{\theta(x,t+T) - \theta(x,t)}{T} = -185.0 + \frac{2\pi}{0.025} \doteq 66.33.$$

The corresponding period is $2\pi/\Omega \doteq 0.095$. It is worth a mention that this solution $A(x,t)$ very well agrees with the following analytic solution to Eqs. (1, 2) obtained in Takáč [22] by rigorous bifurcation analysis,

$$\begin{gathered} \frac{1}{\varepsilon} e^{i\Omega t} A(x,t) = \\ \sin k_n x - \frac{\varrho |\varepsilon|^2}{32 k_n^2} \sin 3k_n x + \left(\frac{\varrho |\varepsilon|^2}{32 k_n^2} \right)^2 (3 \sin 3k_n x + \sin 5k_n x) + \mathcal{O}(|\varepsilon|^6), \end{gathered} \tag{30}$$

where ε is a complex bifurcation parameter whose square modulus $|\varepsilon|^2 > 0$ measures the smallness of $R - k_n^2 > 0$, $k_n = 2n\pi \neq 0$, $\varrho \equiv \frac{1+i\mu}{1+i\nu}$, and $R + i\Omega$ is related to $|\varepsilon|^2$ by

$$\frac{R + i\Omega - (1+i\nu)k_n^2}{1+i\mu} = \frac{3}{4}|\varepsilon|^2 \left(1 - \frac{\varrho}{32 k_n^2}|\varepsilon|^2 + \mathcal{O}(|\varepsilon|^4) \right). \tag{31}$$

Together with the rotating wave (3), the solution (30) bifurcates from the zero solution as R increases past k_n^2.

As the time t increases past 1.29, also this separable periodic orbit shows its instability. For $1.29 \le t \le 1.43$ we observe a connection orbit from this periodic orbit towards a rotating wave (3) with $n = -1$, see Fig. 12(a,b). This rotating wave is identical (up to multiplication by a complex unit reflecting a phase shift) with the one we have started from at $t = 0$. Again, our simulations show

$$|A(x,t)| = 12.063 \quad \text{for all} \quad x \in [0,1] \ \text{ and } \ t \in [1.43, 1.91].$$

From this point on the entire scenario repeats as we have just described it. This can also be seen from the complex plots of the zeroth and first Fourier modes of the function $|A(x,t)|^2$

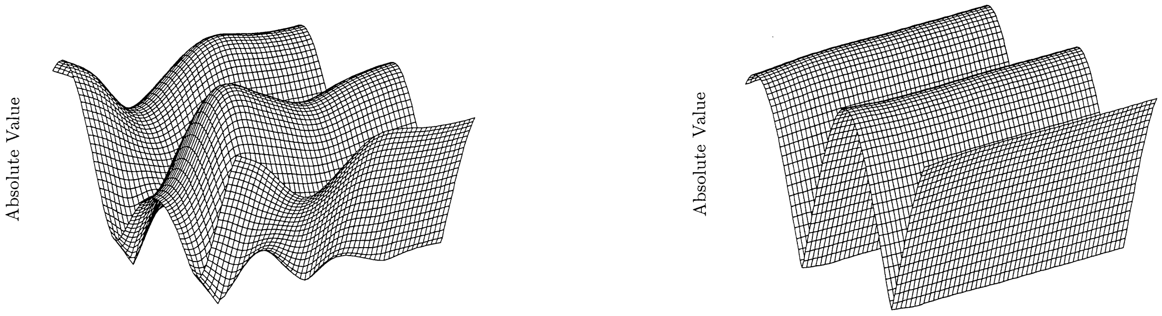

Figure 10: For $R = 185.0$, the modulus $|A(x,t)|$ for (a) $1.00 \le t \le 1.05$; (b) $1.05 \le t \le 1.10$.

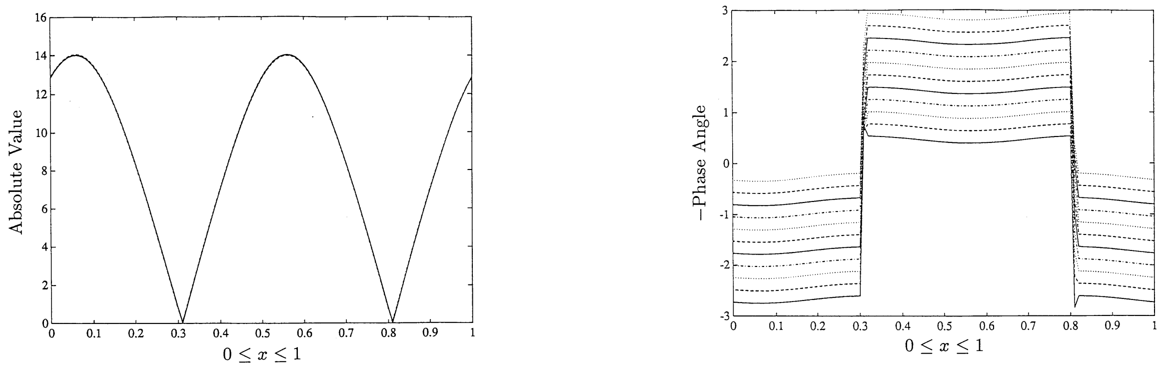

Figure 11: For $R = 185.0$, (a) modulus for $1.06 \le t \le 1.29$; (b) negative phase angle for $1.09 \le t \le 1.10$.

of $x \in [0,1]$, see Fig. 13(a,b). It takes a time interval of (approximate) length 1.55 units for this scenario to repeat.

It is somewhat amazing that the scenario repeats after approximately the same time interval. This fact strongly suggests that our numerical simulations have produced a homoclinic periodic orbit (of period $T = 1.55$) which *shadows* three heteroclinic connection orbits, the first one running from the rotating wave (3) ($n = -1$) towards the 2-torus (23), the second one running from this 2-torus towards the periodic orbit (30), and the third one returning from this periodic orbit towards the rotating wave (3) ($n = -1$). Furthermore, even if we have started our simulations from $A(x, t_0)$ near the rotating wave (3) with $n = 1$, the simulated shadowing periodic orbit has never returned to this rotating wave again. We are unable to explain why our approximating dynamical system "prefers" the rotating wave (3) with $n = -1$ to the one with $n = 1$. Notice that the approximating dynamical system uses the same number of positive and negative complex Fourier modes $e^{ik_n x}$, $|n| \le N$, for the

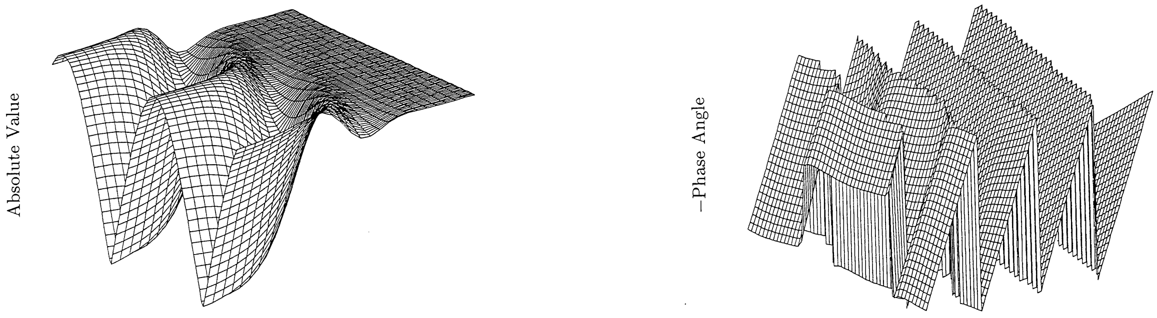

Figure 12: A connection orbit for $R = 185.0$ and $1.30 \leq t \leq 1.40$, (a) modulus; (b) negative phase angle.

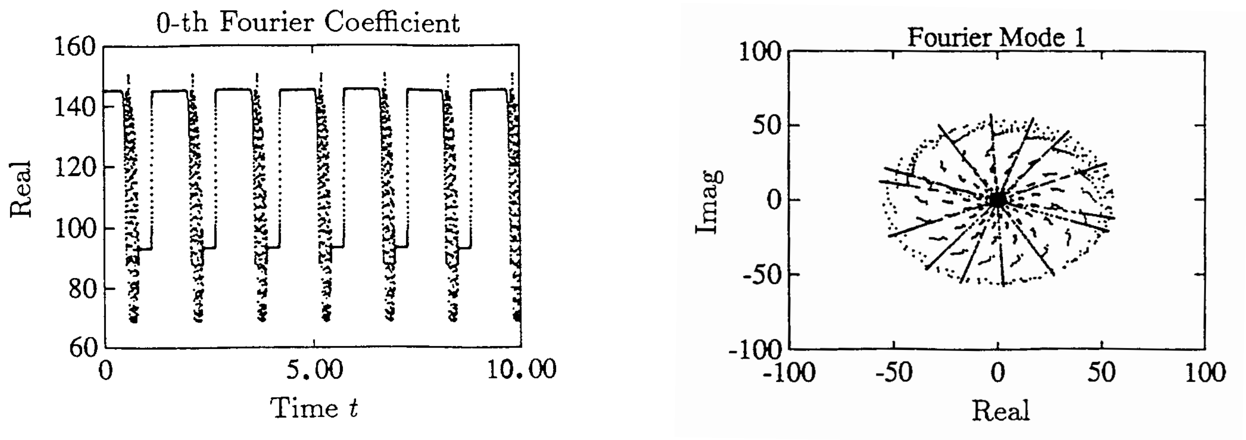

Figure 13: For $R = 185.0$ and $0 \leq t \leq 10.0$, (a) zeroth Fourier mode (real, on vertical axis) versus time (on horizontal axis); (b) first Fourier mode (complex plot) of the square modulus $|A(x,t)|^2$.

spatial approximation, i.e. $A(x,t)$ is approximated by the truncated FOURIER series

$$A_N(x,t) = \sum_{|n| \leq N} c_n(t) e^{ik_n x}. \tag{32}$$

In particular, the corresponding truncation of Eq. (1) yields a system of $2N+1$ ordinary differential equations (ODE's, for short) for $c_n(t)$, $t \geq 0$, cf. DOELMAN [3]. Thus, the only possible reason for $n = -1$ being preferred to $n = 1$ we can think of are some round-off computer errors, despite of double precision complex arithmetics used in our computations. In any event, the *local attractor* $\mathcal{A}$ suggested by our simulations must be symmetric with respect to the reflection $x \mapsto -x$ (i.e. $n \mapsto -n$) because it contains the periodic orbit (30) having this reflection symmetry, and this periodic orbit is connected to all, the 2-torus (23) and the rotating waves (3) with $n = \pm 1$.

More precisely, given the symmetries of the CGL equation, we have obtained a local attractor $\mathcal{A}$ consisting of

(i) two 1D manifolds (circles) $\mathcal{A}'_{\infty}$ and $\mathcal{A}'_{-\infty}$ of rotating waves (3) for $n = \pm 1$, respectively;

(ii) a 3D manifold (a 3-torus) $\mathcal{A}''$ of 2-tori (23);

(iii) a 2D manifold (a 2-torus) $\mathcal{A}'''$ of separable periodic orbits (30); and

(iv) manifolds of connection orbits, $C'_{\pm 1}$, C'' and $C'''_{\pm 1}$. Here, $C'_{\pm 1}$ connects from $\mathcal{A}'_{\pm\infty}$ to $\mathcal{A}''$ and has real dimension 3, C'' connects from A'' to A''' and has 3D, and $C'''_{\pm 1}$ connects from $\mathcal{A}'''$ to $\mathcal{A}'_{\pm\infty}$ and has 2D.

4.2 A local attractor for $R = 250.0$

This case is a simplification of the previous one from §4.1. Again, our simulations start from an initial distribution $A(x, t_0)$ near the rotating wave (3), where $n = 1$, $k_1 = 2\pi$,

$$|a_1| = (250.0 - (2\pi)^2)^{1/2} \doteq 14.51, \tag{33}$$

and $\omega_1 = -250.0 + 6 \cdot (2\pi)^2 \doteq -13.13$. After a transient time interval of about 2 units we set t to $t = 0$ and begin our observations. For $0 \leq t \leq 0.005$, the modulus $|A(x,t)|$ stays within the interval $(14.4, 14.6)$ for all $x \in [0,1]$, see Fig. 14(a). Examining also the phase angle $\theta(x,t)$ from (26) in Fig. 14(b), we conclude that $A(x,t)$ is very close (with relative precision $< 1\%$) to the rotating wave (3) with $n = -1$, for all $t \in [0, 0.005]$, see (33). However, Fig. 14(a,b) suggest that an unstable 2-torus may be present. This 2-torus may be the reason why the computed orbit does not get closer to the rotating wave.

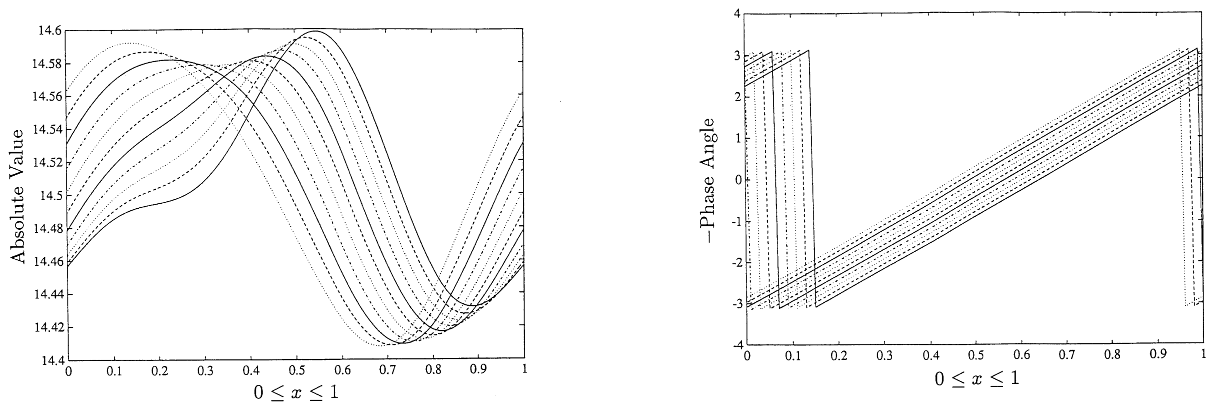

Figure 14: For $R = 250.0$ and $0 \leq t \leq 0.005$, (a) modulus; (b) negative phase angle.

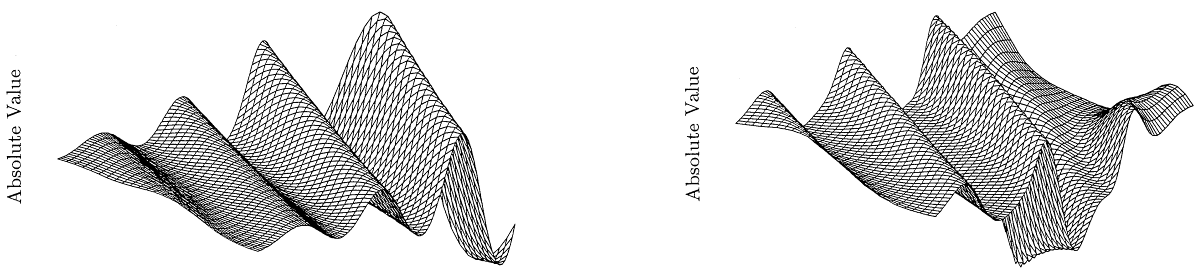

Figure 15: For $R = 250.0$, the deviations $|A(x,t)| - 14.5$ for (a) $0 \le t \le 0.05$; (b) $0.05 \le t \le 0.10$.

As the time t increases past 0.005, we observe both spatial and temporal deviations of $|A(x,t)| - 14.5$ from 0 forming an increasing travelling wave with a sine-like shape moving from the right of the left with the velocity $c_1 = -50$ (approximately), see Fig. 15(a,b). The deviations continue to increase up to $t = 0.085$ when a phase slip occurs at $x = 0.51$ where $A(x,t) = 0$. In this case we observe no sign of $A(x,t)$ approaching a 2-torus (23). Rather, after the phase slip occurs, $A(x,t)$ starts approaching a periodic orbit having the form (30), see Fig. 16(a,b). The modulus $|A(x,t)|$ remains temporally constant for all $t \in [0.23, 0.25]$. Moreover, in (29) we have $|\varepsilon| = 17$ and

$$\Omega = \omega_0 - \frac{\theta(x,t+T) - \theta(x,t)}{T} = -250.0 + \frac{2\pi}{0.025} \doteq 1.33.$$

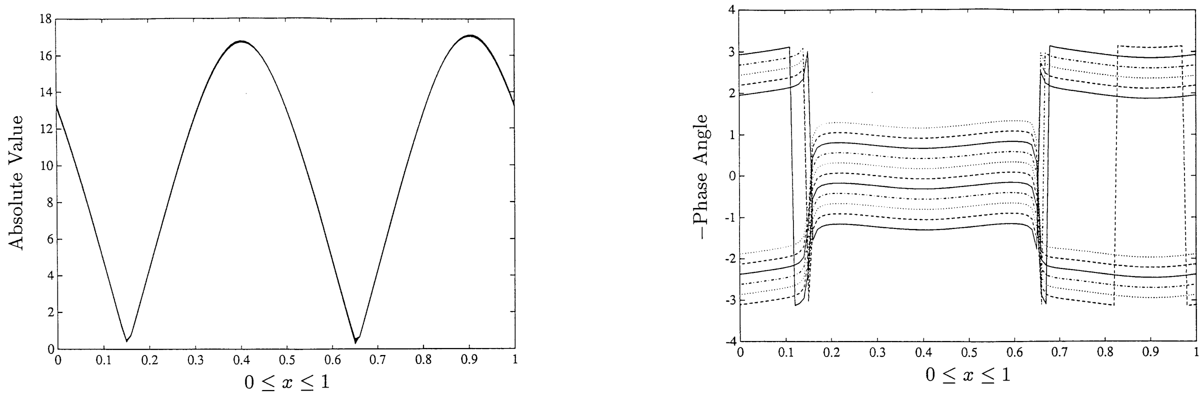

Figure 16: For $R = 250.0$, (a) modulus for $0.23 \le t \le 0.25$; (b) negative phase angle for $0.24 \le t \le 0.25$.

As the time t increases past 0.25, also this separable periodic orbit shows its instability. For $0.25 \le t \le 0.315$ we observe a connection orbit from this periodic orbit towards a rotating wave (3) with $n = -1$, see Fig. 17(a,b). This rotating wave is identical (up to multiplication

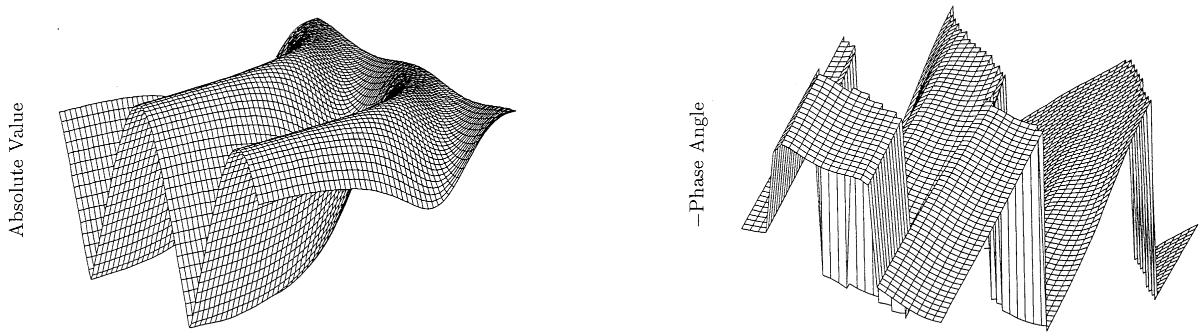

Figure 17: A connection orbit for $R = 250.0$ and $0.25 \leq t \leq 0.30$, (a) modulus; (b) negative phase angle.

by a complex unit reflecting a phase shift) with the one we have started from at $t = 0$. Again, our simulations show

$$\big||A(x,t)| - 14.5\big| < 0.1 \quad \text{for all} \quad x \in [0,1] \ \text{ and } \ t \in [0.315, 0.320].$$

From this point on the entire scenario repeats as we have just described it. This can also be seen from the complex plots of the zeroth and first FOURIER modes of the function $|A(x,t)|^2$ of $x \in [0,1]$. It takes a time interval of (approximate) length 0.316 units for this scenario to repeat.

Given the symmetries of the CGL equation, we have obtained a local attractor $\mathcal{A}$ consisting of

(i) two 1D manifolds (circles) $\mathcal{A}'_{\infty}$ and $\mathcal{A}'_{-\infty}$ of rotating waves (3) for $n = \pm 1$, respectively;

(ii) a 2D manifold (a 2-torus) $\mathcal{A}''$ of separable periodic orbits (30); and

(iii) four 2D manifolds of connection orbits, $C'_{\pm 1}$ and $C''_{\pm 1}$. Here, $C'_{\pm 1}$ connects from $\mathcal{A}'_{\pm\infty}$ to $\mathcal{A}''$, and $C''_{\pm 1}$ connects from $\mathcal{A}''$ to $\mathcal{A}'_{\pm\infty}$.

4.3 Separable periodic orbits for $R = 300.0$ and $R = 350.0$

Both these cases are analogous to the case $R \in (R_I, R_{II}) = (128.3049, 162.4)$ from §3.1. The separable periodic orbits (19) have the angular frequencies $\Omega = -161.30$ for $R = 300.0$ and $\Omega = -257.87$ for $R = 350.0$. The shape of their modulus $|A(x)|$ and the phase angle $|\theta(x)|$ from (26) suggest that these periodic orbits should lie on the same bifurcation branch of separable periodic orbits as those in §3.1.

To summarize the results of this section, for each $R = 185.0$ and 250.0, we have found an interesting local attractor $\mathcal{A}$. For $R = 185.0$, $\mathcal{A}$ consists of two 1D manifolds (circles) of rotating waves (3) for $n = \pm 1$, a 3D manifold (a 3-torus) of 2-tori (23), a 2D manifold (a 2-torus) of separable periodic orbits (30), and manifolds of connection orbits. For $R = 250.0$, $\mathcal{A}$ consists of two 1D manifolds (circles) of rotating waves (3) for $n = \pm 1$, a 2D manifold (a 2-torus) of separable periodic orbits (30), and four 2D manifolds of connection orbits.

5 Discussion

For the supercritical bifurcation at $R = R_{sup} = 137.90$ we have obtained a stable 2-torus for $137.9 < R < 139.7$. For the subcritical bifurcation at $R = R_{sub}$ our results are qualitatively similar to the experimental and numerical results obtained by Janiaud et al. [8, 9] who observed a 2-torus given by Eq. (5) persisting for long time before it collapsed. We have observed its instability outside the tiny interval $84.97 < R < 84.99$; the stability for $R = 84.98$ may be due to numerical errors, cf. (12).

Finally, the numerical simulations studying the stability of the 2-tori having the forms (5) and (23) suggest that these 2-tori may bifurcate into (possibly unstable) 3-tori having the following form,

$$A(x,t) = B(x - ct, t/\tau)e^{-i\Omega t}, \quad -\infty < x < \infty,\ t \geq 0, \tag{34}$$

where $c \neq 0$, $\Omega \neq 0$, $\tau > 0$, and $B(x, \xi)$ is 1-periodic in both $x, \xi \in \mathbb{R}$. Namely, given the symmetries of the CGL equation, the 2-tori (23) form a 3D manifold which itself is a 3-torus (25) invariant under the semiflow generated by Eqs. (1, 2). Hence, it is very reasonable to expect the possibility of a bifurcation that preserves this 3-torus, but the 2-tori (23) bifurcate into a *triperiodic motion* (34). In particular, inserting (34) into (1) we obtain the following boundary value problem for the unknown $(1,1)$-periodic complex-valued function $B(x, \xi)$,

$$\tau^{-1}\partial_\xi B - (1 + i\nu)\partial^2_{xx} B - c\partial_x B - (R + i\Omega)B = -(1 + i\mu)|B|^2 B, \quad x, \xi \in \mathbb{R}. \tag{35}$$

Here, suitable values for the real constants $\mu \neq 0$, $\nu \neq 0$, $\tau > 0$, $c \neq 0$, $R > 0$, and $\Omega \neq 0$ are to be found so that Eq. (35) admits a $(1,1)$-periodic solution $B(x,t)$ such that its modulus $|B(x,t)|$ is nonconstant in both x and t. A different 3-torus motion was obtained in Moon et al. [14] by numerical simulations.

References

[1] **Blennerhassett, P. J.** : *On the generation of waves by wind.* Philos. Trans. Roy. Soc. London, Ser. A, **298**, 451–494 (1980)

[2] **Doelman, A.** : *Slow time-periodic solutions to the Ginzburg-Landau equation.* Physica D **40**(2), 156–172 (1989)

[3] **Doelman, A.** : *Finite-dimensional models of the Ginzburg-Landau equation.* Nonlinearity **4**(2), 231–250 (1991)

[4] **Doering, C. A., Gibbon, J. D., Holm, D. D.** and **Nicolaenko, B.** : *Low-dimensional behaviour in the complex Ginzburg-Landau equation.* Nonlinearity **1**(2), 279–309 (1988)

[5] **Eckhaus, W.** : *Studies in Nonlinear Stability Theory.* Berlin 1965

[6] **Ginzburg, V. L.** and **Landau, L. D.** : *On the theory of superconductivity.* Zh. Eksp. Teor. Fiz. (USSR) **20**, 1064 (1950) English transl. in: Ter Haar, D. (ed.): *Men of Physics: L. D. Landau.* Vol. I, pp. 546–568. New York 1965

[7] **Guckenheimer, J.** and **Holmes, P.** : *Nonlinear Oscillations, Dynamical Systems, and Bifurcations of Vector Fields.* New York 1983

[8] **Janiaud, B., Guyon, E., Bensimon, D.** and **Croquette, V.** : *Sideband instability waves with periodic boundary conditions.* In: Busse, F. H. and Kramer, L. (eds.): *Nonlinear Evolution of Spatio-Temporal Structures in Dissipative Continuous Systems.* NATO ASI Series B; pp. 45–50. New York 1990

[9] **Janiaud, B., Pumir, A., Bensimon, D., Croquette, V., Richter, H.** and **Kramer, L.** : *The Eckhaus instability for travelling waves.* Physica D **55**(3&4), 269–286 (1992)

[10] **Keefe, L. R.** : *Dynamics of perturbed wavetrain solutions to the Ginzburg-Landau equation.* Stud. Appl. Math. **73**, 91–153 (1985)

[11] **Kuramoto, Y.** : *Phase dynamics of weakly unstable periodic structures.* Prog. Theor. Phys. **71**(6), 1182–1196 (1984)

[12] **Kuramoto, Y.** and **Tsuzuki, T.** : *On the formation of dissipative structures in reaction-diffusion systems.* Prog. Theor. Phys. **54**(3), 687–699 (1975)

[13] **Landman, M. J.** : *Solutions of the Ginzburg-Landau equation of interest in shear flow transition.* Stud. Appl. Math. **76**, 187–237 (1987)

[14] **Moon, H. T., Huerre, P.** and **Redekopp, L. G.** : *Transitions to chaos in the Ginzburg-Landau equation.* Physica D **7**(1-3), 135–150 (1983)

[15] **Newell, A. C.** : *Envelope equations.* Lectures in Appl. Math. **15**, 157–163 (1974)

[16] **Newell, A. C.** : *The dynamics of patterns: A survey.* In: Wesfreid, J. E., Brand, H. R., Manneville, P., Albinet, G. and Boccara, N.: *Propagation in Systems Far from Equilibrium.* pp. 122–155. Berlin 1988

[17] **Newell, A. C.** and **Whitehead, J. A.** : *Finite bandwidth, finite amplitude convection.* J. Fluid Mech. **38**(2), 279–303 (1969)

[18] **Newton, P. K.** and **Sirovich, L.** : *Instabilities in the Ginzburg-Landau equation: periodic solutions.* Quart. Appl. Math. **44**(1), 49–58 (1986)

[19] **Newton, P. K.** and **Sirovich, L.** : *Instabilities in the Ginzburg-Landau equation II. Secondary bifurcation.* Quart. Appl. Math. **44**(2), 367–374 (1986)

[20] **Sirovich, L.** and **Newton, P. K.** : *Periodic solutions of the Ginzburg-Landau equation.* Physica D **21**(1), 115–125 (1986)

[21] **Stuart, J. T.** and **Di Prima, R. C.** : *The Eckhaus and Benjamin-Feir resonance mechanisms.* Proc. Roy. Soc. London Ser. A **362**, 27–41 (1978)

[22] **Takáč, P.** : *Invariant* 2*-tori in the time-dependent Ginzburg-Landau equation.* Nonlinearity **5**(2), 289–321 (1992)

received: September 6, 1995

Author:

Prof. Dr. Peter Takáč, Ph.D.
Fachbereich Mathematik
Universität Rostock
Universitätsplatz 1
D–18055 Rostock, Germany
e-mail: peter.takac@mathematik.uni-rostock.de